ORIGINAL PAPER

Romano Rinaldi · G. D. Gatta · G. Artioli
K. S. Knight · C. A. Geiger

Crystal chemistry, cation ordering and thermoelastic behaviour of CoMgSiO$_4$ olivine at high temperature as studied by in situ neutron powder diffraction

Abstract The thermal expansion, structural changes and the site partitioning of Co and Mg in synthetic CoMgSiO$_4$ olivine have been studied by in situ time-of-flight neutron powder diffraction as a function of temperature, between 25 and 1,000°C. Thermal expansion of the unit cell dimensions and volume are linear within this temperature range and give no indications of a phase transition, although the thermoelastic behaviour indicates a slight strain minimum around 700°C. Co^{2+} shows a strong preference for the M1 site throughout this temperature range with an oscillatory behaviour; it decreases slightly at about 300°C, climbing up to nearly its original value at around 800°C and then decreasing by about 30% at 1,000°C. This behaviour is in contrast with that of (Fe, Mg)$_2$SiO$_4$ olivine, in which the initial Fe^{2+} site preference for the M1 site switches to the M2 site beyond a cross-over temperature. The oscillatory site preference in (CoMg)-olivine as a function of temperature is reflected in the M–O polyhedral volume changes and M–O bond lengths, as well as, thermoelastic strain and atomic thermal displacement parameters. The imbalance between the increasing vibrational and decreasing configurational entropy contributions, together with covalent bonding effects rather than crystal field contributions, seem to drive the cation partitioning in (CoMg)-olivine.

R. Rinaldi (✉)
Dipartimento di Scienze della Terra,
Università di Perugia, 06100 Perugia, Italy
E-mail: rrinaldi@unipg.it

G. D. Gatta · G. Artioli
Dipartimento di Scienze della Terra,
Università di Milano, 20133 Milano, Italy
E-mail: diego.gatta@unimi.it

K. S. Knight
ISIS Facility, Rutherford Appleton Laboratory,
Chilton, Didcot, Oxon OX11 0QX, UK

K. S. Knight
Department of Mineralogy, The Natural History Museum,
Cromwell Road, London, SW7 5BD, UK

C. A. Geiger
Mineralogisch-Petrographisches Institut der Christian Albrechts
Universität, Kiel, Germany

Introduction

In situ neutron diffraction studies on different (Fe, Mg)$_2$SiO$_4$ olivine compositions (Rinaldi and Wilson 1996; Rinaldi et al. 2000; Redfern et al. 2000) indicate an unusual Mg–Fe partitioning behaviour as a function of temperature. With increasing temperature, natural mantle olivines (Fa$_{12}$Fo$_{88}$, Fa$_{10}$Fo$_{90}$) show an initial tendency towards ordering with Fe^{2+} preferring the octahedral M1 site at lower temperatures, followed by a temperature region of disorder and finally, through a cross-over temperature of about 900°C, a switchover to anti-ordering with Fe^{2+} strongly preferring the octahedral M2 site between above 900 and 1,300°C. A similar behaviour was also observed in a synthetic sample of composition Fa$_{50}$Fo$_{50}$, where the initial ordering with Fe^{2+} preference for the M1 site, is more pronounced than in the mantle samples in response to kinetic effects during synthesis and the cross-over temperature (with switchover to anti-ordering) is lowered to about 650°C, in accordance with a higher Fe^{2+} content. Such anti-ordered modifications can be expected to persist up to the melting temperature. These in situ studies provided the first direct experimental confirmation of theoretical predictions (Akamatsu and Kumazawa 1993) that Fe–Mg exchange reactions in olivine are effectively non-quenchable due to very rapid kinetics. The monitoring of olivine's structural behaviour as a function of temperature and composition was achieved thanks to the high crystallographic resolution offered by neutron diffraction and the recent developments of time-of-flight (TOF) techniques allowing the simultaneous collection

Table 1 Experimental and instrumental parameters pertaining to the Rietveld refinement

Instrumental diffractometer	POLARIS (neutron TOF powder diffract.)
Flight path	12.7837 m
Detector	ZnS scintillator–216 elements, $2\theta = 90°$
2θ range	$83° < 2\theta < 97°$
Temperatures	20, 300, 600, 800, 1,000°C
Refinement	
Space group	*Pbnm*
Z	4
Unit cell refinement	Whole pattern
Observations	4,879
Refined parameters	38 total
Structural	18
Profile	2
Background	10
Cell	3
Constraints	$X_{Co}(M1) + X_{Mg}(M1) = 1$, $X_{Co}(M2) + X_{Mg}(M2) = 1$, $X_{Co}(M1) = X_{Mg}(M2) = 1 - X_{Mg}(M1) = 1 - X_{Co}(M2)$
Thermal parameters	All atoms isotropic
Agreement factors	$wRp(20°C) = 0.046$; $wRp(300°C) = 0.046$; $wRp(600°C) = 0.043$; $wRp(800°C) = 0.044$; $wRp(1000°C) = 0.045$

of diffraction data from a wide range of reciprocal space and under non-ambient conditions. Further similar studies by in situ high-T neutron diffraction, were devoted to the temperature dependence of cation ordering in synthetic (Fe, Mn)- and (Mg, Mn)-olivines (Redfern et al. 1997) and in (Ni, Mg)-olivines (Henderson et al. 2001). These studies showed that the behaviour of the (Ni, Mg)-olivines on disordering is significantly different from that of the (Fe, Mn) and (Mg, Mn) samples. In particular, the non-convergent ordering of the (Ni, Mg)-olivines is controlled by the strong affinity of Ni for the M1 site, and only at $T > 800°C$ the samples show a progressive, but slight, decrease in order. In contrast, in (Fe, Mn)- and (Mg, Mn)-olivines Mn shows a preference for the M2 site at low T, and becomes increasingly disordered over the two sites at $T > 500°C$.

This paper reports an in situ high temperature neutron diffraction study of the olivine composition CoMgSiO$_4$, in which Co^{2+} shows a strong energetic preference for the M1 site (Ghose and Wan 1974; Müller-Sommer et al. 1997). Through the Co–Mg intersite partitioning and the thermoelastic behaviour of the olivine structure as a function of temperature, we wish to

further investigate the crystal-chemical and physical constraints determining the non-ideal behaviour of the olivine solid solution as a function of temperature and cation substitution.

Experimental

The Mg–Co olivine was synthesised from high purity oxides that were sintered (Co_3O_4 at 350°C for 24 h; MgO and SiO_2 at 1,100°C for 24 h) to drive off any adsorbed water and organic impurities. The oxides were mixed in proportion for the CoMgSiO$_4$ composition, ground and mixed with water in an agate mortar to obtain a fine homogeneous powder. The powder was pressed into 10 mm diameter pellets, which were then sintered in three cycles for 48 h and reground between each sintering. The first two cycles were done at 1,200°C and the third at 1,300°C. The final product was polycrystalline and pinkish red in colour. An X-ray diffraction pattern measured over 24 h showed sharp reflections that could be indexed to olivine with no major impurities. A 50 mm long cylinder of 7 mm

Table 2 Unit-cell parameters, thermal expansion coefficients and unit-strain ellipsoid parameters of CoMgSiO$_4$ at different temperatures

T (°C)	a (Å)	b (Å)	c (Å)	V (Å^3)
20	4.77572(8)	10.27159(17)	6.00235(10)	294.441(6)
300	4.78873(8)	10.30879(18)	6.02484(11)	297.423(7)
600	4.80159(10)	10.34656(18)	6.04592(11)	300.361(7)
800	4.81065(10)	10.37135(20)	6.06168(12)	302.435(8)
1000	4.82045(11)	10.39863(23)	6.07821(11)	304.677(8)
α (°C^{-1})	$9.5(1) \times 10^{-6}$	$12.5(1) \times 10^{-6}$	$12.7(2) \times 10^{-6}$	$3.51(4) \times 10^{-5}$

T-T_0 (°C)	$\varepsilon 1$ (°C^{-1})$\times 10^5$	$\varepsilon 2$ (°C^{-1})$\times 10^5$	$\varepsilon 3$ (°C^{-1})$\times 10^5$	$\varepsilon 1$:$\varepsilon 2$:$\varepsilon 3$
280	1.34(2)	1.29(2)	0.972(8)	1.38:1.33:1.0
580	1.26(2)	1.23(2)	0.934(8)	1.35:1.32:1.0
780	1.27(2)	1.24(2)	0.938(7)	1.35:1.32:1.0
980	1.29(3)	1.26(2)	0.956(8)	1.35:1.32:1.0

Table 3 Structural data for CoMgSiO$_4$ at different temperatures

	x	y	Z	Site occupancy	K_D	Uiso $\times$ 100
T = 20°C						
M1	0	0	0	0.698(9) (Co)	5.34(48)	0.278(4)
M2	0.9912(5)	0.27708(19)	0.25	0.302(9) (Co)		0.507(3)
Si	0.42513(33)	0.09485(20)	0.25	1.0		0.385(3)
O1	0.76762(33)	0.09247(14)	0.25	1.0		0.556(2)
O2	0.21814(34)	0.44846(12)	0.25	1.0		0.542(2)
O3	0.27961(22)	0.16408(11)	0.03348(16)	1.0		0.595(1)
T = 300°C						
M1	0	0	0	0.684(10) (Co)	4.68(46)	0.868(6)
M2	0.9899(6)	0.27732(22)	0.25	0.316(10) (Co)		0.886(5)
Si	0.4256(4)	0.09517(23)	0.25	1.0		0.635(3)
O1	0.7667(4)	0.09342(18)	0.25	1.0		1.082(3)
O2	0.2163(4)	0.44893(15)	0.25	1.0		1.067(3)
O3	0.27897(27)	0.16389(13)	0.03391(19)	1.0		1.111(2)
T = 600°C						
M1	0	0	0	0.690(11) (Co)	4.95(54)	1.287(8)
M2	0.9880(6)	0.27787(25)	0.25	0.310(11) (Co)		1.358(6)
Si	0.4257(4)	0.09582(25)	0.25	1.0		1.001(4)
O1	0.7656(4)	0.09386(20)	0.25	1.0		1.497(4)
O2	0.2173(4)	0.44962(17)	0.25	1.0		1.623(4)
O3	0.27975(30)	0.16435(15)	0.03417(21)	1.0		1.580(3)
T = 800°C						
M1	0	0	0	0.694(12) (Co)	5.14(62)	1.308(9)
M2	0.9874(7)	0.28007(28)	0.25	0.306(12) (Co)		1.814(8)
Si	0.4250(5)	0.09449(28)	0.25	1.0		1.201(5)
O1	0.7643(5)	0.09452(22)	0.25	1.0		1.703(5)
O2	0.2178(5)	0.44985(20)	0.25	1.0		1.979(5)
O3	0.28001(34)	0.16484(17)	0.03481(25)	1.0		2.008(4)
T = 1,000°C						
M1	0	0	0	0.659(14) (Co)	3.73(50)	1.773(12)
M2	0.9875(9)	0.27961(33)	0.25	0.341(14) (Co)		2.268(10)
Si	0.4249(5)	0.09516(31)	0.25	1.0		1.518(5)
O1	0.7640(5)	0.09441(25)	0.25	1.0		2.242(6)
O2	0.2171(5)	0.45040(22)	0.25	1.0		2.325(6)
O3	0.2801(5)	0.16480(20)	0.03503(26)	1.0		2.233(4)

The Co content of M1, Xco(M1), is given. $X_{Co}(M1) = X_{Mg}(M2) = 1 - X_{Mg}(M1) = 1 - X_{Co}(M2)$

diameter pellets was used for the neutron data collection. It was suspended in the vacuum chamber of the high temperature furnace by a thin Ta wire and held in a Ta wire mesh basket.

Neutron powder diffraction data were collected using the Polaris TOF instrument at the ISIS pulsed spallation neutron source of the Rutherford Appleton Laboratory (UK). The instrument uses a "white" beam with neutron wavelengths ranging between 0.7 and 5.1 Å and a primary flight path of 12.784 m. Instrumental parameters are the same as reported by Redfern et al. (2000), with slightly different experimental parameters due to the nature of the sample and the use of a furnace with a tantalum, rather than vanadium, heating element. Diffraction data used in the structure refinement were collected at 20, 300, 600, 800, and 1,000°C by the detector bank placed at 90° from the forward scattering direction and covering the TOF range of 1.7–19.5 ms. This corresponds to a *d*-spacing ranging between 0.37 and 4.26 Å for a total of 4,879 data points per histogram of the powder diffraction patterns. Suitable collimation of the incident and scattered beams made contamination of the diffraction pattern by signals from the sample environment apparatus negligible. Data collections were carried out over periods of 350 µAh at room temperature and 300°C and 400 µAh at all subsequent temperatures. Equilibration periods of 0.5 h were allowed between the end of one measurement and the beginning of the next. Assessment of the temperature log files showed the next set-point was reached within 5 min of finishing a run. After data collection at 1,000°C, the next experiment, planned for 1,300°C, could not be carried out, because the olivine started to melt.

Structure refinements

Crystal structure refinements were carried out using the GSAS Rietveld refinement software (Larson and Von Dreele 1997) in space group *Pbnm* starting with the structure model of Ghose and Wan (1974). The neutron scattering lengths were taken from the GSAS library. Scale factor, background (modelled by Chebyschev polynomials), cell parameters and peak profile (exponential pseudo-Voigt convolution, profile function no. 3 in GSAS, Von Dreele 1990, unpublished) were refined first. The refinements of the atomic parameters (position, occupancy and isotropic thermal displacement)

Table 4 Bond lengths (Å) and angles (°) of CoMgSiO$_4$ as a function of temperature

Bond lengths (Å) and angles (°)	T (°C)				
	25	300	600	800	1,000
M1–O1 (×2)	2.0942(11)	2.1083(13)	2.1201(14)	2.1315(16)	2.1372(18)
M1–O2 (×2)	2.0842(11)	2.0957(13)	2.0973(14)	2.0999(16)	2.1059(18)
M1–O3 (×2)	2.1596(11)	2.1635(13)	2.1768(15)	2.1867(17)	2.1916(19)
< M1–O >	2.113	2.123	2.131	2.139	2.145
M2–O1	2.1762(27)	2.1764(34)	2.1830(40)	2.2040(40)	2.2070(50)
M2–O2	2.0673(26)	2.0749(31)	2.0905(35)	2.0810(40)	2.0920(50)
M2–O3 (×2)	2.2211(19)	2.2313(24)	2.2459(26)	2.2607(30)	2.2627(35)
M2–O3′ (×2)	2.0693(15)	2.0769(17)	2.0759(19)	2.0742(22)	2.0825(25)
< M2–O >	2.137	2.145	2.153	2.159	2.165
Si–O1	1.6358(24)	1.6333(29)	1.6322(32)	1.6320(40)	1.6340(42)
Si–O2	1.6520(24)	1.6536(28)	1.6612(31)	1.6501(40)	1.6541(41)
Si–O3 (×2)	1.6364(14)	1.6400(17)	1.6420(19)	1.6494(22)	1.6493(24)
< Si–O >	1.640	1.642	1.644	1.645	1.647
O1–M1–O2′ (×2)	93.35(5)	93.16(6)	93.23(7)	93.17(7)	93.20(8)
O1–M1–O2 (×2)	86.65(5)	86.84(6)	86.77(7)	86.83(7)	86.80(8)
O1–M1–O3′ (×2)	95.33(5)	95.56(7)	95.61(7)	95.77(8)	95.76(9)
O1–M1–O3 (×2)	84.67(5)	84.44(7)	84.39(7)	84.23(8)	84.24(9)
O2–M1–O3 (×2)	74.45(4)	74.22(4)	74.12(5)	74.09(6)	73.90(7)
O2–M1–O3′ (×2)	105.55(4)	105.78(4)	105.88(5)	105.91(6)	106.10(7)
O1–M2–O3 (×2)	81.31(7)	81.27(9)	81.3(1)	80.9(1)	81.0(1)
O1–M2–O3′ (×2)	90.85(8)	90.88(9)	90.9(1)	90.4(1)	90.4(1)
O2–M2–O3 (×2)	96.89(7)	97.0(1)	96.7(1)	96.6(1)	96.8(2)
O2–M2–O3′ (×2)	90.42(7)	90.30(9)	90.5(1)	91.3(1)	91.1(1)
O3–M2–O3‴(×2)	88.53(3)	88.52(4)	88.29(4)	87.99(5)	88.02(5)
O3–M2–O3′	71.62(8)	71.4(1)	71.0(1)	70.5(1)	70.5(1)
O3–M2–O3″	110.6(1)	110.9(1)	111.7(2)	112.7(2)	112.6(2)
O1–Si–O2	113.6(1)	113.6(2)	113.7(2)	114.6(2)	114.2(2)
O1–Si–O3 (×2)	115.54(8)	115.6(1)	115.6(1)	115.0(1)	115.2(1)
O2–Si–O3 (×2)	102.69(8)	102.6(1)	102.6(1)	103.1(1)	102.9(1)
O3–Si–O3′	105.2(1)	105.1(1)	105.3(2)	104.5(2)	104.8(2)

were based on the stoichiometric composition CoMg-SiO$_4$. Therefore, the fractional populations of Co and Mg in the M1 and M2 sites were refined according to the following formulation: $X_{Co}(M1) + X_{Mg}(M1) = 1$, $X_{Co}(M2) + X_{Mg}(M2) = 1$, $X_{Co}(M1) = X_{Mg}(M2) = 1 - X_{Mg}(M1) = 1 - X_{Co}(M2)$. No stereochemical constraints were used for the bond distances and no preferred orientation correction was applied. Table 1 reports the experimental and instrumental parameters pertaining to the Rietveld refinement. Figure 1 and Table 2 show the unit-cell parameters and their changes as a function of temperature. Table 2 also reports the thermal expansion coefficients and unit strain ellipsoid parameters at various temperatures. Convergence was rapidly achieved after the first few cycles of refinement. In the final cycles the shifts in all parameters were less than their standard deviations.

To avoid errors in the atomic occupancies due to correlation with the atomic displacement (thermal) parameters, three different tests were made: first, by a close inspection of the terms of the variance–covariance matrix, then by alternately fixing thermal and occupancy parameters. Finally, a fixed value of the thermal parameters was adopted for both M-sites at each temperature (obtained by a linear regression of the averages of the U_{iso} values of both M sites at each temperature) and the site occupancies and all other structural parameters were refined. The refinements of all the three

tests converged towards the same final values. Even at the highest temperature, the refined occupancy factors differed by less than 1.5σ from those obtained in the unconstrained refinements. This demonstrates the absence of significant correlation effects between site occupancies and thermal parameters. As a matter of fact, thanks to the coverage of a wide range of scattering vectors, which results from the neutron scattering cross-section (Q independence of scattering intensity), neutron diffraction enables the separation of the information on thermal motion from that of site occupancy in structure refinements (Rinaldi 2002; Dove 2002). Table 3 reports the structural data of CoMgSiO$_4$ for the five-structure refinements as a function of temperature. Relevant bond lengths and angles are listed in Table 4. Observed and calculated diffraction patterns at 20 and 1,000°C are shown in Fig. 2.

Table 5 M1 and M2 polyhedral volumes as a function of temperature

T (°C)	V_{M1} (Å^3)	V_{M2} (Å^3)
20	11.91(2)	12.53(2)
300	12.20(2)	12.65(2)
600	12.26(3)	12.78(2)
800	12.48(2)	12.85(3)
1,000	12.57(3)	12.96(3)

Results

Thermoelastic behaviour

The variation of the lattice parameters of $CoMgSiO_4$ with temperature (Fig. 1) is continuous and the data show no anomalies that may be related to a phase transition. The axial and volume thermal expansion coefficient $[\alpha_j = l_j^{-1}(\partial l_j / \partial T), \ \alpha_V = V^{-1}(\partial V / \partial T)]$ were calculated by weighted linear regression through the data points (Fig. 1, Table 2), and yield the following values: $\alpha_a = 9.5(1) \times 10^{-6}$, $\alpha_b = 12.5(1) \times 10^{-6}$, $\alpha_c = 12.7(2) \times 10^{-6}$, $\alpha_V = 3.51(4) \times 10^{-5} °C^{-1}$. The thermal expansion of $CoMgSiO_4$ is strongly anisotropic $(\alpha_a : \alpha_b : \alpha_c = 1.00 : 1.32 : 1.34)$, and is consistent with earlier observations on isostructural (Mg, Fe)-olivines (Smyth et al. 2000).

The magnitudes of the principal unit-strain coefficients $(\varepsilon_1, \varepsilon_2, \varepsilon_3)$, between room temperature and each measured T, and the orientations of the strain ellipsoids (Table 2) were calculated with the software STRAIN (Ohashi 1982). The unit strain ellipsoid is oriented with $\varepsilon_1 || c$, $\varepsilon_2 || b$, $\varepsilon_3 || a$ and $\varepsilon_1 > \varepsilon_2 > \varepsilon_3$, as shown in Fig. 3. The evolution of the unit-strain coefficients with temperature in both, Co–Mg and Fe–Mg olivines are shown in Fig. 4a and b. In (Co, Mg)-olivine, the magnitude of all three unit-strain coefficients decreases slightly with T, reaching a slight minimum at about 700°C, then slightly increases again with increasing temperatures. The lowest value corresponds with the maximum in the X_{Co} (M1) (Fig. 5, Table 3). However, each trend appears to be continuous. The thermoelastic anisotropy, calculated on the basis of the unit-strain parameters between T_0 and each measured T, is nearly constant within the T-range investigated. The maximum anisotropy is observed between 20 and 300°C, with $\varepsilon_1 : \varepsilon_2 : \varepsilon_3 = 1.38 : 1.33 : 1.00$; for all the other temperatures $\varepsilon_1 : \varepsilon_2 : \varepsilon_3 = 1.35 : 1.32 : 1.00$ (Table 2). The thermoelastic anisotropy of $CoMgSiO_4$ calculated on the basis of the unit-strain coefficients is very high and is in good agreement with the thermal expansion anisotropy $(\alpha_a : \alpha_b : \alpha_c = 1.00 : 1.32 : 1.34)$. In contrast, in the case of Fe–Mg olivines, two of the three unit-strain coefficients $(\varepsilon_1$ and $\varepsilon_2)$ have similar values at HT (Fig. 4b). This represents an increase in the thermoelastic anisotropy with T, an opposite trend with respect to the isomorphic (Co, Mg)-olivines.

HT-structural evolution

The most significant crystallographic parameters were analysed in terms of their temperature-induced varia-
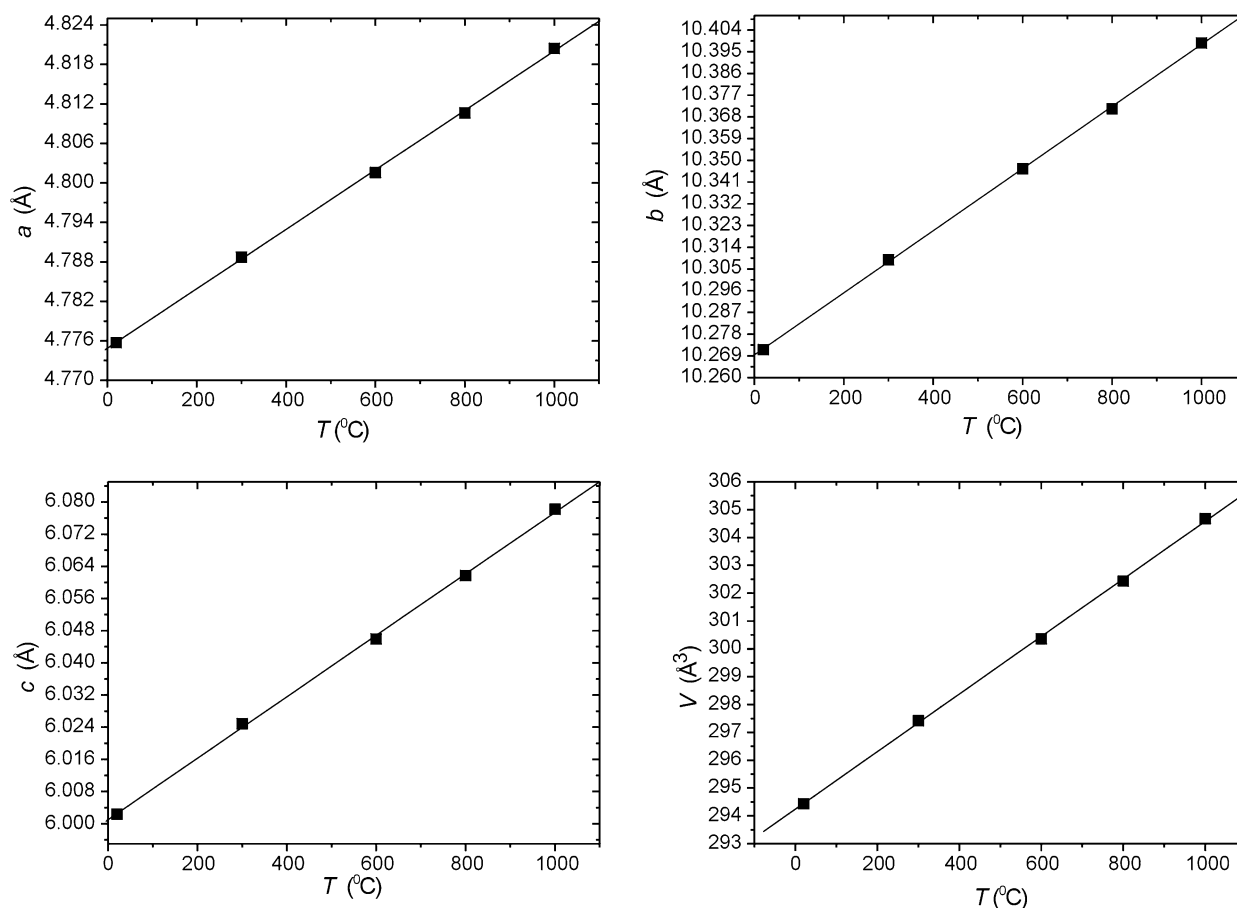

Fig. 1 Evolution of cell parameters of $CoMgSiO_4$ as a function of temperature. *Solid lines* are weighted linear fits through the data. The estimated standard deviations are smaller than the size of the symbols

Fig. 2 Experimental (*crosses*) and calculated (*solid line*) TOF neutron diffraction pattern for CoMgSiO$_4$ at 20°C (*above*) and 1,000°C (*below*). Calculated peak positions and difference plots are shown at the *bottom* of each pattern
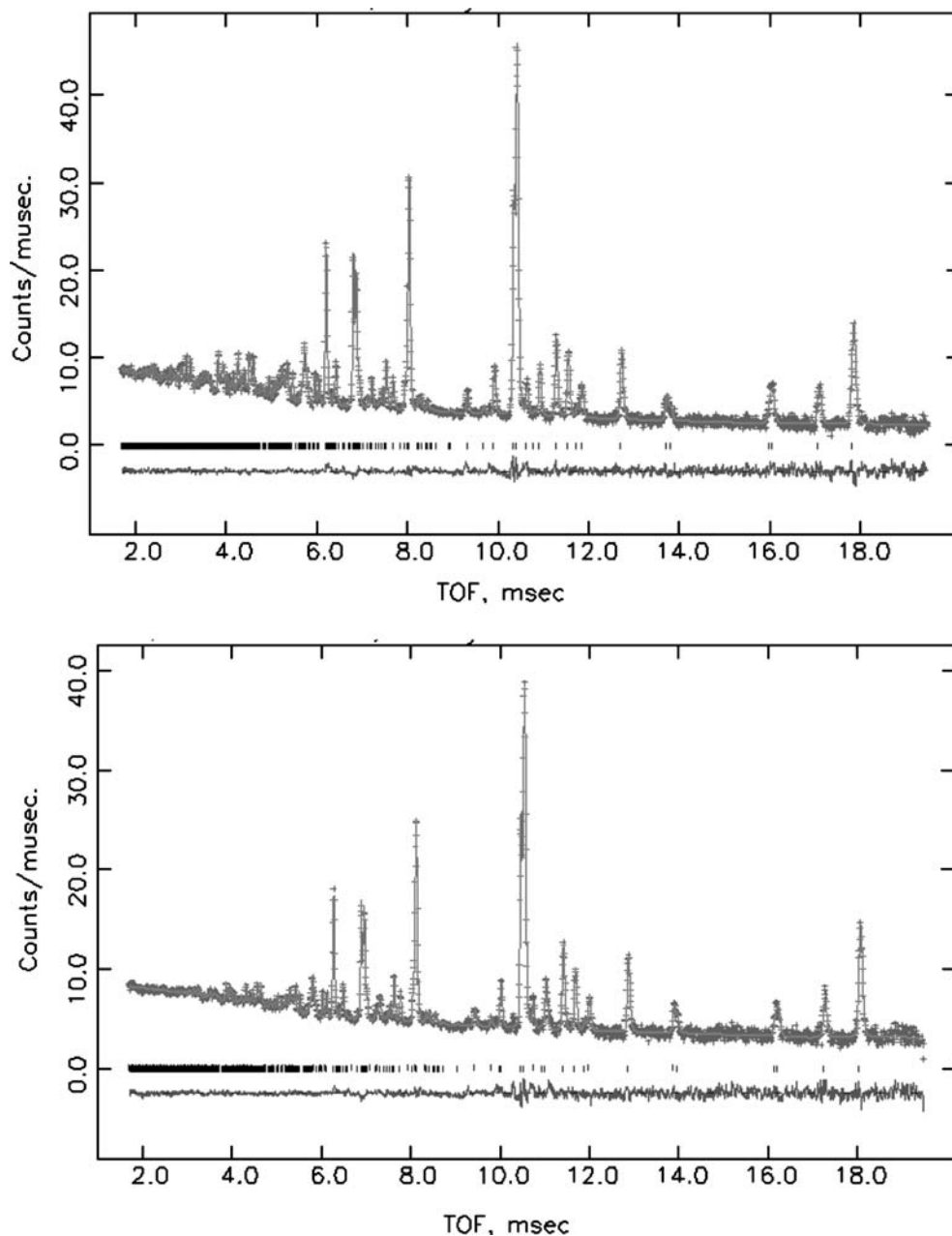
tions. These include: atomic positions, angles and bond distances, site occupancies of the two octahedral cations (Co and Mg) in the M1 and M2 sites, atomic displacement parameters of the two M sites, octahedral volumes, M–O bond distances, O–M–O angles and *T*-induced polyhedral strain.

The degree of cation ordering, determined from direct measurements of site occupancies in the two octahedral M sites, can be described by the equilibrium constant of the cation exchange reaction, K_D expressed as:

$$K_D = \frac{[Co(M1) \times Mg(M2)]}{[Co(M2) \times Mg(M1)]}.$$

Values of K_D above 1 represent a state of ordering, with Co preferring the M1 site and Mg the M2 site. The value of $K_D = 1$ represents the state of total disorder. The results (Fig. 5) show that Co has a strong preference for the M1 site at *RT* ($K_D = 5.3$), which is virtually maintained up to 800°C ($K_D = 5.1$), despite the gradual heating of the sample over a considerable length of time (up to ~15 h). A slight oscillation in K_D with temperature, although within the error bar, can be appreciated with a noticeable dip around 300°C ($K_D = 4.7$). A decrease in ordering (30% of the initial value) occurs at 1,000°C ($K_D = 3.7$). It should be noted that even at this high temperature and over a long heating time, the degree of ordering is high, indicating the possibility of a high degree of ordering up to the melting temperature. In view of the careful refinement procedure adopted to avoid correlations between site occupancies and thermal

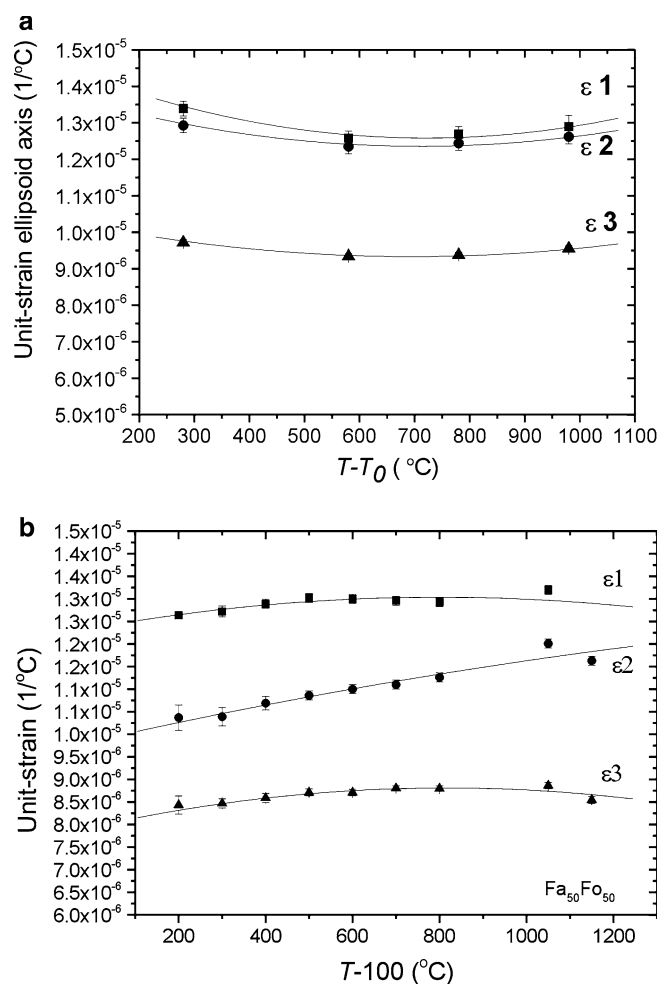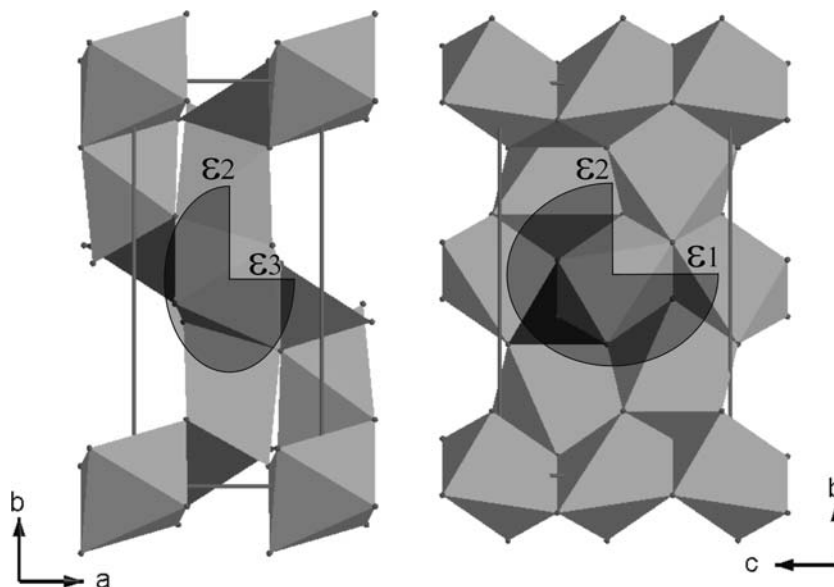**Fig. 3** Orientation of the thermal unit-strain ellipsoid in CoMgSiO$_4$ olivine

Fig. 4 a Magnitude of the three principal unit-strain coefficients in CoMgSiO$_4$ olivine calculated as $T-T_0$, where T is the temperature of interest and T_0 is 20°C. *Solid lines* represent weighted quadratic fits to the data. **b** Unit-strain ellipsoid axis versus $T-100$°C in MgFeSiO$_4$ olivine, calculated from the cell parameters reported in Redfern et al. (2000)

parameters of cations in the octahedral sites, these values of site occupancies can be treated with a good degree of confidence.

The slight oscillatory behaviour of the site occupancies in the plot of cation partitioning versus temperature (Fig. 5) is reflected in the polyhedral volume variations, especially for M1 (Fig. 6, Table 5). The thermal expansion regimes of the two M sites (Fig. 7) show that M1, with a much less regular thermal expansion regime than M2, on average, shows a higher rate of thermal expansion. A similar behaviour is observed in MgFeSiO$_4$ (Redfern et al. 2000). The average M–O bond lengths of the two polyhedral sites increase linearly with temperature, with a slight tendency to converge at high temperature, in accordance with the decrease in ordering at 1,000°C (Fig. 8). The polyhedral strain, calculated according to Ghose and Wan (1974) (Fig. 9, Table 6), indicates a higher total strain (longitudinal + shear strain) rate for M2 than for M1 as a function of temperature. However, the polyhedral strain plot also shows a higher total strain for M1, due to the strong distortion of the M1 polyhedron hosting Co^{2+}. In contrast, the M2 polyhedron appears to be more regular. This result is in agreement with Ghose and Wan (1974).

The thermal displacement parameters (Fig. 10) show a slightly divergent behaviour for the two M sites between the temperatures of 600 and 800°C. This temperature interval corresponds with the slight kink in site occupancy, with the minimum in the thermoelastic strain and with the kink in thermal expansion regime of the M1 polyhedron (Fig. 7).

Discussions

This study provides detailed information on the response of the octahedral site geometry to temperature in Co–Mg olivine in the temperature range between *RT*
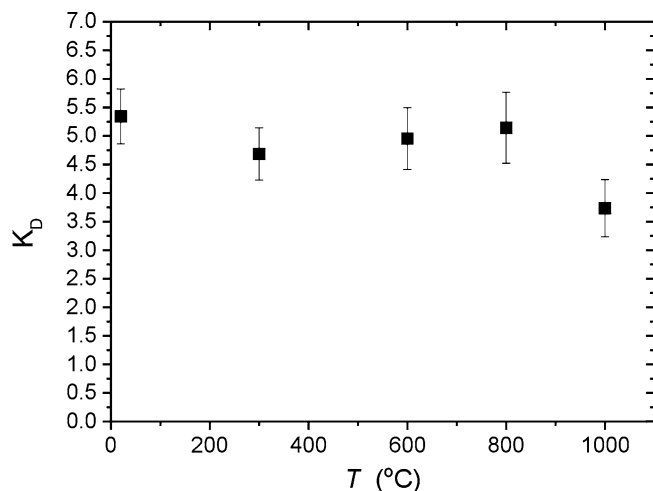
Fig. 5 Cation distribution for Co and Mg in M1 and M2 expressed as K_D versus temperature in CoMgSiO$_4$. The *horizontal line* represents disorder

Fig. 7 Thermal expansion behaviour of the M1 and M2 sites in CoMgSiO$_4$: evolution of the polyhedral volumes normalised to the room temperature values (V_0)

and 1,000°C. Comparison of the present results with those obtained for natural and synthetic Fe–Mg olivines has implications for the segregation from the melt of transition metals and on their crystal chemical behaviour. The ordering reversal observed in Fe–Mg olivines is not present in the Co–Mg variety which shows a much stronger cation segregation (with Co in M1 and Mg in M2). Co^{2+}, despite its larger ionic size than that of Mg^{2+} ($^{VI}R_{Co^{2+}} = 0.745$, $^{VI}R_{Mg^{2+}} = 0.720$, Shannon 1976), has a marked preference for the M1 site even at high temperatures. The reasons for this site-preference have been addressed by Ghose and Wan (1974). They argued that the energetics associated with covalent bonding between the *d*-orbitals of the cobalt cation and the *sp*³-orbitals of the oxygen anions prevail over an ionic size-driven preference for the octahedral sites involved. Considerations by the same authors on the crystal field theory (site distortion criterion) and site preference in olivines as compared to pyroxenes carried the conclusion that crystal field stabilization energy (CFSE) effect alone is incapable of explaining the
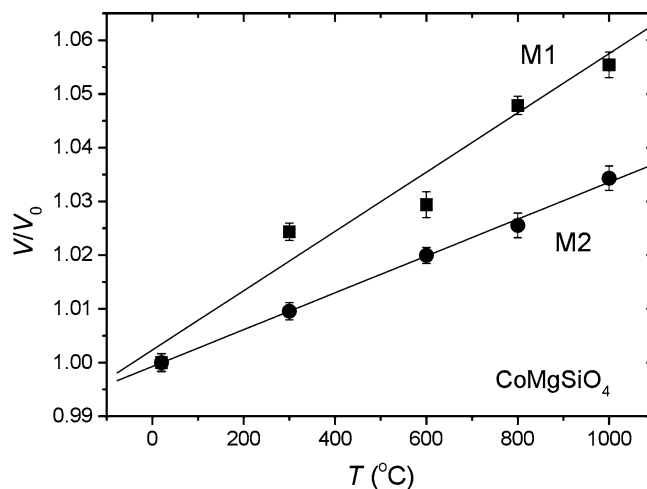
partitioning of Co and Mg in the two M sites (Ghose and Wan 1974). Similar arguments by the same authors explained the essential lack of ordering found in natural Fe, Mg-olivines as a result of the mutual neutralization of the two competing effects (covalent bonding and ionic size) for the Fe^{2+} and Mg^{2+} cations. The larger Co^{2+} ion would therefore show a preference for the smaller (and more distorted) M1 site owing to the stronger covalent bonding available at this site rather than at M2. Furthermore, such ordering is seen here to be strong in the synthesised Co–Mg-olivine, to persist at high temperature and to presumably be retained up to the melting point. Heating of the sample up to 800°C over a period of approximately 15 h reveals the persistence of the same degree of ordering as that found at *RT*, after a slight decrease at lower temperatures (between 300 and 600°C). Indeed, the cation order of a slowly cooled sample of the same composition used in the present study, corresponds to an estimated equilibrium temperature of 800°C in Müller-Sommer et al. (1997).
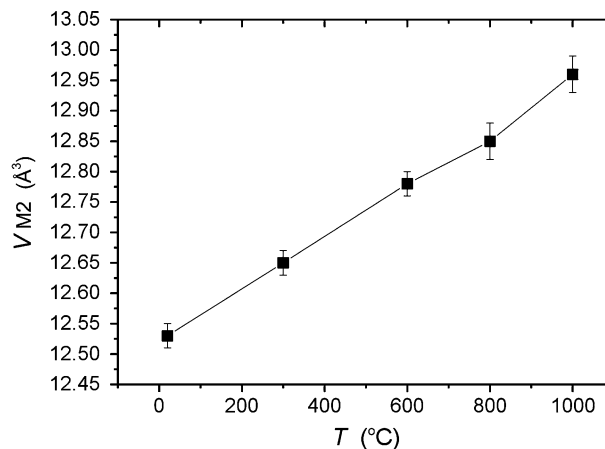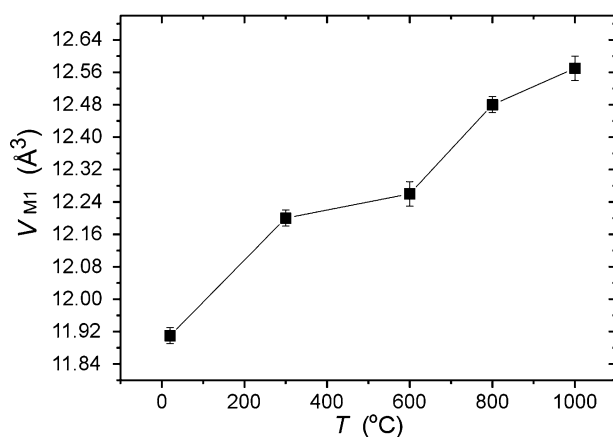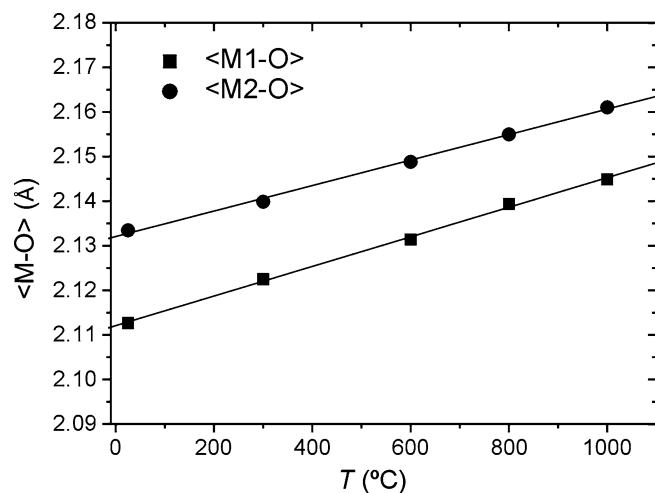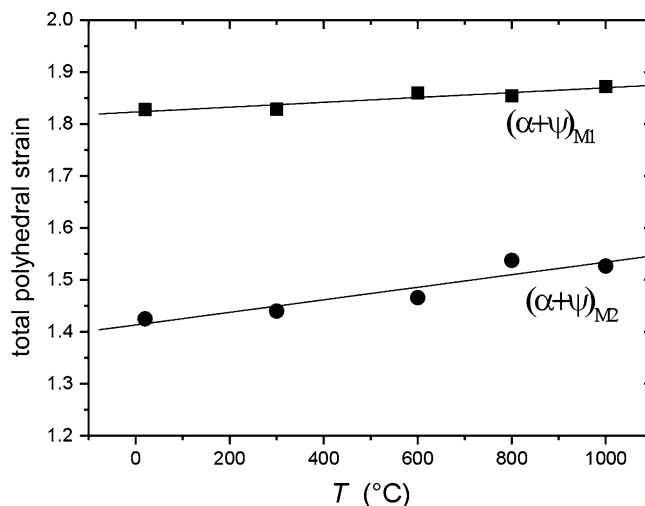

Fig. 6 M1 and M2 polyhedral volumes as a function of temperature in CoMgSiO$_4$ olivine

Table 6 Distortion of M1 and M2 octahedra at different temperatures

T (°C)	M1 $|\alpha|$	M1 $|\psi|$	M1 total strain	M2 $|\alpha|$	M2 $|\psi|$	M2 total strain
20	0.10757	1.72038	1.82795	0.07336	1.35176	1.82795
300	0.08749	1.74135	1.82884	0.07456	1.36556	1.82884
600	0.10262	1.75727	1.85989	0.07671	1.38914	1.85989
800	0.08933	1.76520	1.85453	0.08230	1.45528	1.85453
1,000	0.09048	1.78166	1.87214	0.08164	1.44525	1.87214

A comparison among the *HT* behaviours of (Co, Mg)-olivines and (Fe, Mn)-, (Mg, Mn)- and (Ni, Mg)-olivines shows that Co and Ni lead to a similar non-convergent ordering of Mg and Ni/Co over the M1 and M2 sites at *HT*. In contrast, Mn shows a preference for the M2 site in both (Fe, Mn)- and (Mg, Mn)-olivines at $T < 500°C$ and becomes increasingly disordered at $T > 500°C$, following a specific equilibrium disordering path. This behaviour is due to the similar strong affinity of Ni and Co for the M1 site and, as inferred by several authors (Burns 1970; Wood 1974; Ghose and Wan 1974; Bish 1981; Tsukimura and Sasaki 2000; Henderson et al 2001), such affinity is not tied to ionic size effects. In addition, Ghose and Wan (1974) stated that the site preference for M1 site in olivine follows the order $Ni^{2+} > Co^{2+} > Fe^{2+}$. In contrast, the structural adjustments accompanying the ordering of Fe–Mn and Mg–Mn over the M1 and M2 sites in (Fe, Mn)- and (Mg, Mn)-olivines are more likely to be controlled by ionic size effects (Redfern et al. 1997; Henderson et al. 2001).

The diverging trends of the atomic displacement parameters (U_{iso}) for the two cations (Co and Mg) is analogous to that found in Fe–Mg olivines, Fa_{10}, Fa_{12} and Fa_{50} (Rinaldi et al. 2000; Redfern et al. 2000), although the much stronger preference of Co^{2+} for the M1 site (as compared with that of Fe^{2+} for the same site) hinders occupancy or U_{iso} cross-over with temper-

Fig. 9 Polyhedral strain in $CoMgSiO_4$ calculated according to Ghose and Wan (1974)

ature that occurs in the three Fe–Mg olivines investigated earlier. Such behaviour can be ascribed, also in the case of the Co–Mg composition, to vibrational rather than static effects (Rinaldi et al. 2000; Redfern et al. 2000).

The main deformation mechanism with T of the M1 and M2 polyhedra, due to O–M–O angle variations (Table 4), gives rise to a high anisotropy in thermal expansion: the O1–M1–O3′ and O2–M1–O3′ angles increase by ~0.5% between 25 and 1,000°C, the O2–M2–O3′ angle by ~0.7% and the O3–M2–O3″ by ~1.8%. In contrast, O1–M1–O3, O2–M1–O3 and O3–M2–O3‴ angles decrease by less than 0.8% and O3–M2–O3′ by ~1.5% within the same *T*-range. These mechanisms mainly act on the expansion of b and c with T and, therefore, lead to a high difference in axial thermal expansion coefficients ($\alpha_c > \alpha_b > \alpha_a$).

Fig. 8 Average bond lengths for the M1 and M2 sites versus T in $CoMgSiO_4$
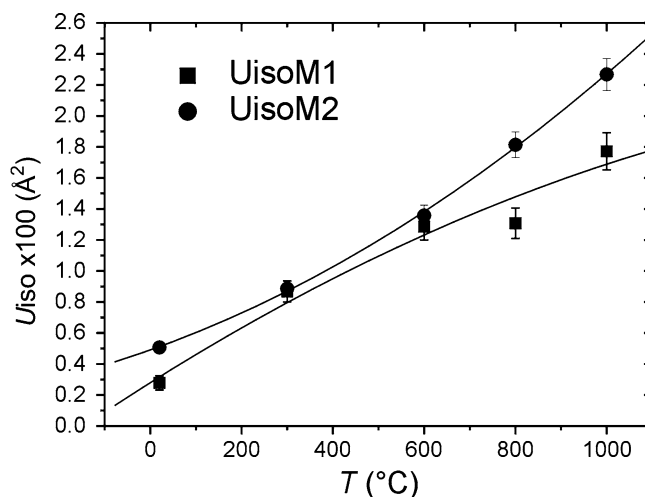
Fig. 10 Atomic displacement parameters for the M1 and M2 sites as a function of temperature. *Solid lines* are weighted quadratic fits to the data

References

Akamatsu T, Kumazawa M (1993) Kinetics of intracrystalline cation redistribution in olivine and its implications. Phys Chem Miner 19: 423–430

Bish DL (1981) Cation ordering in synthetic and natural Ni-Mg olivine. Am Mineral 66: 770–776

Burns RG (1970) Mineralogical application of crystal field theory. Cambridge University Press, Cambridge, p 224

Dove MT (2002) An introduction to the use of neutron scattering methods in mineral sciences. Eur J Mineral 14/2: 203–224

Ghose S, Wan C (1974) Strong site preference of Co^{2+} in olivine $Co_{1.10}Mg_{0.90}SiO_4$. Contrib Mineral Petrol 47: 131–140

Henderson CMH, Redfern SAT, Smith RI, Knight KS, Charnock JM (2001) Composition and temperature dependence of cation ordering in Ni-Mg olivine solid solutions: a time-of-flight neutron powder diffraction and EXAFS study. Am Mineral 86:1170–1187

Larson AC, Von Dreele RB (1997) GSAS: general structure analysis system. Document LAUR 86–748, Los Alamos National Laboratory, New Mexico, USA

Müller-Sommer M, Hock R, Kirfel A (1997) Rietveld refinement study of the cation distribution in (Co, Mg)-olivine solid solution. Phys Chem Miner 24: 17–23

Ohashi Y (1982) STRAIN, a program to calculate the strain tensor from two sets of unit-cell parameters. In: Hazen RM, Finger LW (eds) Comparative crystal chemistry. Wiley, New York, pp 92–102

Redfern SAT, Henderson CMB, Knight KS, Wood BJ (1997) High temperature order-disorder in $(Fe_{0.5}Mn_{0.5})_2SiO_4$ and $(Mn_{0.5}Mg_{0.5})_2SiO_4$ olivines: an in situ neutron diffraction study. Eur J Mineral 9: 287–300

Redfern SAT, Artioli G, Rinaldi R, Henderson CMB, Knight KS, Wood BJ (2000) Octahedral cation ordering in olivine at high temperature. II: P an in situ neutron powder diffraction study on synthetic $MgFeSiO4$ (Fa50). Phys Chem Miner 27: 630–637

Rinaldi R (2002) Neutron scattering in mineral sciences. Eur J Mineral 14/2: 195–202

Rinaldi R, Artioli G, Wilson CC, McIntyre G (2000) Octahedral cation ordering in olivine at high temperature. I: in situ neutron single crystal diffraction studies on natural mantle olivines (Fa12 and Fa10). Phys Chem Miner 27: 623–629

Rinaldi R, Wilson CC (1996) Crystal dynamics by neutron time-of-flight Laue diffraction in olivine up to 1573 K using single frame methods. Sol State Commun 97/5: 395–400

Smyth JR, Jacobsen SD, Hazen RM (2000) Comparative crystal chemistry of orthosilicate minerals. In: Hazen RM, Downs RT (eds) High-temperature and high-pressure crystal chemistry. Reviews in Mineralogy and Geochemistry, vol. 41, Mineralogical Society of America and Geochemical Society, Washington, DC, pp 187–210

Shannon RD (1976) Revised effective ionic radii and systematic studies of interatomic distances in halides and chalcogenides. Acta Cryst A32: 751–767

Tsukimura K, Sasaki S (2000) Determination of cation distribution in (Co,Ni,Zn)$_2$SiO$_4$ olivine by synchrotron X-ray diffraction. Phys Chem Miner 27:234–241

Wood BJ (1974) Crystal field spectra of Ni^{2+} in olivine. Am Mineral 59: 244–248